sustainability

Article

Thermal Performance Optimization of Multiple Circuits Cooling System for Fuel Cell Vehicle

Hao Huang [1,2], Hua Ding [1], Donghai Hu [1,*], Zhaoxu Cheng [1], Chengyun Qiu [1], Yuran Shen [3] and Xiangwen Su [2]

1 School of Automobile and Traffic Engineering, Jiangsu University, Zhenjiang 212013, China
2 CATARC Automotive Test Center (Changzhou) Co., Ltd., Changzhou 213161, China
3 Automobile Engineering Research Institute, Nanjing Automobile (Group) Corporation, Nanjing 210028, China
* Correspondence: 1000004735@ujs.edu.cn

Abstract: Due to its advantages of high efficiency, high power density at low temperature, fast start-up and zero emission, fuel cells are of great significance in automobile drive application. A car powered by electricity generated by an on-board fuel cell device is called a fuel cell vehicle (FCV). Fuel cells have a large demand for heat dissipation, and the layout space of automotive cooling modules is limited. Based on this situation, a parallel arrangement of multiple radiators is proposed. Using numerical simulation means to verify and optimize the designed multiple circuits cooling system (MCCS), from the original layout scheme based on the Taguchi method to establish the objective function of the reliability design of the MCCS, select A2/B1/C1/D2/E1/F1. In the scheme, the outlet temperature of the fuel cell is finally reduced to 75.8 °C. The cooling performance is improved, and the spatial layout of the individual cooling components can also be optimized. The whole vehicle experiment was carried out under four working conditions of full power idling charging, half power idling charging, constant speed of 40 km/h and constant speed of 80 km/h, to verify the cooling performance of the MCCS and to prove the effectiveness of the MCCS designed in this paper.

Keywords: fuel cell vehicle (FCV); multiple circuits cooling system (MCCS); multiple radiators; thermal performance optimization

Citation: Huang, H.; Ding, H.; Hu, D.; Cheng, Z.; Qiu, C.; Shen, Y.; Su, X. Thermal Performance Optimization of Multiple Circuits Cooling System for Fuel Cell Vehicle. *Sustainability* **2023**, *15*, 3132. https://doi.org/10.3390/su15043132

Academic Editor: Nicu Bizon

Received: 24 December 2022
Revised: 20 January 2023
Accepted: 2 February 2023
Published: 8 February 2023

1. Introduction

As a new energy technology, the fuel cell has many applications [1]. Among them, the fuel cell vehicle (FCV) has the advantages of environmental protection, zero pollution, and high efficiency [2–4]. They are a vehicle of the future and are highly regarded as an electricity source worthy of ongoing focus [5–7]. They have become a current research hotspot [8]. The heat generated by the proton exchange membrane fuel cell (PEMFC) [9] mainly depends on the circulation of the coolant in the cooling system. Temperature is an important parameter affecting the performance of the fuel cell [10–12]. Temperature is also related to the efficiency [13]. Therefore, it is necessary to develop and optimize the cooling system of the FCV. The front cabin cooling system is an important part of the FCV, mainly used to dissipate heat from the PEMFC. Due to the large heat dissipation requirements of the PEMFC and the limited layout space of the vehicle cooling module, it is difficult for the cooling system of the FCV to meet the heat dissipation requirements. Therefore, this paper proposes a parallel arrangement of multiple radiators: separately arranging multiple radiators at positions with good air circulation, which can effectively reduce the volume of single radiators, saves space in the front cabin and meets fuel requirements and performance usage requirements for battery cooling. For the FCV cooling system configuration, Xu et al. [14] established a vehicle-integrated thermal management system, in which two radiators and a condenser are arranged in series. The cooling system is compact and can reduce air resistance but reuse of cooling air results in insufficient heat transfer capacity. Zhang et al. [15] established a one-dimensional simulation model of a 30 kW PEMFC cooling system and used a coupled simulation model to calculate the heat dissipation performance of the cooling system. The results show that the simulation results of heat transfer are in agreement with the experimental data, but the low-temperature cooling system of the stack is the same as the traditional structure, which cannot obtain high heat transfer efficiency. Xing et al. [16] established a PEMFC stack and cooling system model for a new hybrid vehicle model, which ensured that additional PEMFC heat would be removed to stabilize the stack temperature but ignored the PEMFC temperature change and heat dissipation requirements. Zhang et al. [17] established a liquid-driven fan cooling system for a hydrogen fuel cell forklift to ensure that the fluid temperature at the radiator outlet was within the control range. However, when the cooling demand increases, the technical advantages of the cooling system are not obvious. To make up for the shortcomings of the above research, this paper establishes a multiple circuits cooling system (MCCS), which considers the temperature change of the PEMFC outlet water and the heat dissipation requirements, improves the heat exchange capacity of the system, improves the air circulation of the radiator and thus improves the heat exchange efficiency and saves space in the front cabin.

For the thermal performance optimization of the FCV, Zhu et al. [18] studied the simulation analysis of the cooling system for a high-temperature PEMFC used in automotive power and proposed a cooling strategy for optimizing performance. The superposition model was verified according to the experimental results, which show that adjusting the cooling oil flow rate (2.5–5 kg/s) can meet the heat dissipation requirements of the PEMFC stack, but the oil cooling system technology is not mature enough. Philip et al. [19] used a mathematical method based on Pinch Analysis to optimize the thermal management system of the FCV. The research results showed that by using paraffin, the heat dissipation area of the radiator can be greatly optimized and meet the requirements of the vehicle, but the use of this phase change material will increase the cost and body weight. In cooling system control strategy optimization, Fly et al. [20] established a complete set of system simulations and then compared conventional liquid cooling and evaporative cooling fuel cell systems. The results showed that the aluminum condensing evaporative cooling system achieves heat and water balance with a larger frontal area of the radiator than conventional liquid cooling. The system costs 27% less, but the contamination problem of the aluminum heat exchanger and the change of the working fluid from liquid to two-phase requires a redesign of the traditional radiator, which greatly increases the cost. Su et al. [21] proposed a decoupled control strategy and established a pump flow controller, a fuzzy PID fan controller and a Simulink-GT fuel cell cooling system model. The results showed that the control strategy successfully met the heat dissipation requirements of the fuel cell. For PEMFC heat dissipation performance optimization, the MCCS studied in this paper is different from the above-mentioned optimizations. It is a new type of cooling circuit optimization, which can not only improve the cooling performance but also optimize the spatial layout of each cooling component, and the technical difficulty and cost are relatively low.

Aiming at the above problems, this paper has carried out the following research: (a) Propose a MCCS for an FCV, establish a model and analyze the performance of the MCCS simulation; (b) Determine the thermal performance optimization of the MCCS performance based on the Taguchi method. (c) Verify the effectiveness of the MCCS designed in this paper and the correctness of the one-dimensional/three-dimensional simulation through real vehicle experiments.

2. Model Establishment and Thermal Performance Verification

2.1. Temperature Control Structure

The heat dissipation of the FCV depends on the cooperation of various components inside the MCCS. The water-cooled MCCS mainly consists of radiators, water pumps and pipelines (as shown in Figure 1). After the PEMFC stack generates heat, it transfers the heat to the coolant, and the temperature of the coolant rises. The water pump will use on the coolant in the MCCS to promote the circulation of the coolant in the pipeline and control the flow of the coolant. Heat will be carried through the radiator in this circulating flow, and when the coolant flows through the core of the radiator, it will be blown strongly by the cooling fans of each radiator, causing the temperature of the coolant to drop rapidly. The coolant will re-enter the cooling cycle of the PEMFC its temperature is lowered. During this period, the coolant evaporates and decreases due to the high working temperature of the PEMFC, and when it decreases to a certain extent, it will be replenished by the expansion tank. The PEMFC has a suitable working temperature range.

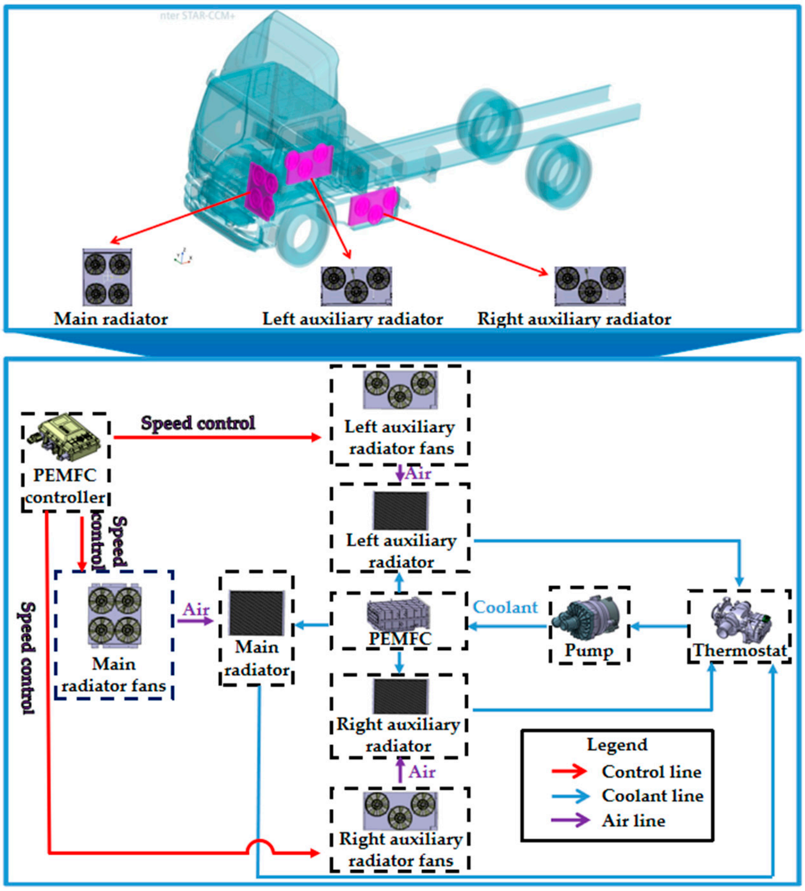

Figure 1. Temperature control structure of PEMFC.

2.2. Thermal Characteristics Model

2.2.1. PEMFC Heating Model

PEMFC heating is mainly caused by the loss of voltage, and its heating value is related to the output current and output voltage. The actual output voltage of the PEMFC is Nernst open circuit voltage after activation polarization loss, concentration polarization loss, and ohmic pole. The actual output voltage of the PEMFC can be expressed as [22–24]:

$$V_{cell} = E_{net} - V_{act} - V_{ohm} - V_{con} \tag{1}$$

In the formula, E_{net} is the Nernst open circuit voltage, V; V_{act} is the activation polarization voltage, V; V_{ohm} is the ohmic polarization voltage, V; V_{con} is the concentration polarization voltage, V.

(1) Nernst Open Circuit Voltage E_{net}

The Nernst open circuit voltage is related to the operating temperature, the partial pressure of oxygen at the cathode and the partial pressure of hydrogen at the anode, and its expression is:

$$E_{net} = 1.229 - 0.85 \times 10^{-4}(T_{st} - 298.15) + 4.3085 \times 10^{-5} T_{st} \ln\left(P_{H_2} P_{O_2}^{0.5}\right) \tag{2}$$

In the formula, T_{st} is the operating temperature of the PEMFC, K; P_{H_2} is the partial pressure of hydrogen at the interface between the anode catalyst and the gas, atm; P_{O_2} is the partial pressure of hydrogen at the interface between the anode catalyst and the gas, atm.

The partial pressure of hydrogen P_{H_2} can be obtained according to the following formula:

$$P_{H_2} = \left(0.5 P_{H_2O}^{sat}\right) \left[\frac{1}{\exp\left(\frac{1.653i}{T_{st}^{1.334}}\right) \frac{\varphi_a P_{H_2O}^{sat}}{P_a}} - 1 \right] \tag{3}$$

In the formula, $P_{H_2O}^{sat}$ is the saturated water vapor pressure, atm; i is the current density, $\mathrm{A/cm^2}$; φ_a is the relative humidity of the anode water vapor (humidification by saturated water vapor, φ_a = 1) and P_a is the anode gas pressure, atm.

The saturated water vapor pressure can be calculated by the following formula:

$$\begin{aligned} \lg P_{H_2O}^{sat} = -2.1794 + 0.02953(T_{st} - 273.15) - 9.1837 \times 10^{-5}(T_{st} - 273.15)^2 \\ +1.4454 \times 10^{-7}(T_{st} - 273.15)^3 \end{aligned} \tag{4}$$

The oxygen partial pressure P_{O_2} can be calculated by the following formula:

$$P_{O_2} = \frac{\left(P_c - \varphi_c P_{H_2O}^{stt}\right)}{1 + \frac{0.79}{0.21}\exp\left(\frac{0.291i}{T_{st}^{0.832}}\right)} \tag{5}$$

In the formula, P_c is the cathode gas pressure, atm; φ_c is the relative humidity of cathode water vapor (humidification by saturated water vapor, φ_c = 1).

(2) Activation Polarization Voltage V_{act}

The activation polarization electromotive force is mainly caused by the sluggish electrochemical rate [25], which can be expressed as:

$$V_{act} = \xi_1 + \xi_2 \cdot T_{amb} + \xi_3 \cdot T_{amb} \cdot (\ln C_{o_2}) + \xi_4 \cdot T_{amb} \cdot (\ln I_{st}) \tag{6}$$

In the formula, C_{o_2} is the oxygen concentration, g/L; ξ_1, ξ_2, ξ_3, ξ_4 are empirical coefficients, T_{amb} is the ambient temperature, K; I_{st} is the output current of the PEMFC, A.

Oxygen concentration C_{o_2} can be calculated by Henry's law [26,27]:

$$C_{O_2} = \frac{P_{O_2}}{5.08 \times 10^6 \cdot \exp(-498/T_{st})} \tag{7}$$

(3) Ohmic Polarization Voltage V_{ohm}

The ohmic polarization electromotive force is mainly caused by the equivalent membrane impedance of the proton exchange membrane [28,29], so it can be expressed by the following formula:

$$V_{ohm} = I_{st} \cdot R_{ohm} \tag{8}$$

In the formula, the expression of the equivalent impedance R_{ohm} of the battery is as follows:

$$R_{ohm} = \frac{l \exp[-350(1/303 - 1/T_{st})]}{-0.003 + 0.0915\varphi_{st} - 0.2048\varphi_{st}^2 + 0.185\varphi_{st}^3} \tag{9}$$

In the formula, l is the thickness of the electrolyte, cm; φ_{st} is the water content of the proton exchange membrane.

(4) Concentration Polarization Voltage V_{con}

The concentration polarization voltage is mainly caused by the high concentration of reactants [29], which can be expressed by the following formula:

$$V_{con} = -\frac{R \cdot T_{st}}{zF} \ln\left(1 - \frac{i}{i_{\max}}\right) \tag{10}$$

In the formula, R is the reaction constant; z is the number of reaction electrons; F is the Faraday constant; i_{max} is the maximum current density, A/cm^2. PEMFC heating is mainly caused by the above-mentioned loss voltage, and its heating value is related to the output current and output voltage. The calculation method of the heating value is shown in the following formula [30]:

$$Q_s = N_{cell} \cdot (E_{net} - V_{cell}) \cdot I_{\mathrm{st}} \tag{11}$$

In the formula, N_{Cell} is the number of PEMFC cells.

2.2.2. MCCS Heat Dissipation Model

There are three main ways to dissipate the heat generated by the PEMFC. Most of the heat is taken away by the coolant [31–33]. The operating temperature of the PEMFC can be expressed as:

$$c_{st} m_{st} \frac{dT_{st}}{dt} = Q_s - Q_{cl} - Q_{amb} \tag{12}$$

In the formula, c_{st} is the average specific heat capacity of the PEMFC, J/(kg·K); m_{st} is the mass of the PEMFC, kg; Q_{cl} is the heat taken away by the coolant, kW; Q_{atm} is the heat exchanged with the environment, kW.

The heat removed by the coolant can be expressed as:

$$Q_{cl} = L_c \cdot C_w \cdot (T_{c,out} - T_{c,in}) \tag{13}$$

In the formula, L_c is the flow rate of the coolant flowing through the PEMFC, kg/s; C_w is the specific heat capacity of the coolant, kJ/(kg·K); $T_{c,out}$ is the outlet temperature of the coolant flowing through the PEMFC, K; $T_{c,in}$ is the inlet temperature of the coolant flowing into the PEMFC, K.

In this study, if the operating temperature of the PEMFC is approximately equal to the outlet temperature of the coolant [34,35], then:

$$Q_{cl} = L_c \cdot C_w \cdot (T_{st} - T_{c,in}) \tag{14}$$

If the heat exchanged between the PEMFC and the external environment is mainly related to the ambient temperature and its own operating temperature, then the heat exchanged with the external environment can be expressed as:

$$Q_{amb} = (T_{st} - T_{amb})/R_t \tag{15}$$

In the formula, R_t is the PEMFC thermal resistance, K/W.

The heating of the PEMFC will affect its working performance; therefore, it is very important to control the temperature of the PEMFC. If the heat is not dissipated in time, the operating temperature of the PEMFC will exceed the safe temperature range, which will not only affect the efficiency of the PEMFC but also cause safety hazards, and the service life of the PEMFC will also be reduced.

2.3. Wind Characteristics Model

2.3.1. Radiator Wind Resistance Model

Air side resistance refers to the resistance encountered when the air is blown in by the fan and flows through the MCCS during the heat dissipation process of the MCCS. The air side resistance of the system mainly comes from the radiator, and the cooling gas flow required by the radiator is [36]:

$$V_a = \frac{Q_{cl}}{\Delta t_a \cdot \gamma_a \cdot c_a} \tag{16}$$

In the formula, Δt_a is the air temperature difference between the inlet and outlet of the PEMFC, °C; γ_a is the density of the coolant in the radiator, kg/m^3; c_a is the specific heat capacity of the coolant in the radiator, J/(kg·K).

The cooling area of the radiator is [37]:

$$F_R = \frac{V_a}{v_a} \tag{17}$$

In the formula, v_a is the air velocity, m/s; V_a is the required air flow rate, cfm.

The air side resistance in the radiator can be calculated by the Formula (18):

$$\Delta P_R = \frac{{V_a}^2}{2\rho_1 A^2}\left[\left(1-\sigma^2+K_c\right)+\frac{4fL}{D_h}\frac{\rho_1}{\rho_m}+2\left(\frac{\rho_1}{\rho_2}-1\right)-\left(1-\sigma^2-K_e\right)\frac{\rho_1}{\rho_2}\right] \tag{18}$$

In the formula, A is the frontal area of the radiator, m^2; ρ_1, ρ_2 are the air inlet and outlet densities of the radiator, kg/m^3; D_h is the equivalent diameter of the air side; ρ_m is the average density of the air in the radiator, kg/m^3; σ is the relative free section; K_c, K_e are the inlet and outlet pressure loss coefficients; f is the surface friction coefficient of the radiator core; L is the internal flow channel length of the radiator, m.

2.3.2. Radiator Cooling Fan Model

The total resistance to be overcome by the cooling fan during work is equal to the sum of the flow resistance of all the components in the air duct, and this model can be described as:

$$\dot{V} = \dot{V}_0 - a(p_r - 1)^{\mathrm{b}} \tag{19}$$

In the formula, V_0 represents the maximum air volume of the fan; p_r is the pressure ratio; b is the pressure rise coefficient.

(1) Air Volume of Fan

The air volume of the fan can be calculated by the Formula (20):

$$V_f = \frac{V_a}{\eta_f} \tag{20}$$

V_f is the air volume of the radiator fan, m^3·s^{-1}; V_a is the cooling air requirement, m^3·s^{-1}; η_f is the volumetric efficiency of the fan, generally 0.7~0.9.

(2) Wind Pressure of Fan

The internal structure of the MCCS radiator is complex, and the fan sucks and rotates behind the radiator, causing a pressure drop after the air flow passes through the radiator. In order for the cooling air to overcome the resistance of the circulation system and pass through the radiator smoothly to achieve the cooling effect, the fan needs to generate a certain pressure. The wind pressure ΔP_f of the fan is determined by the resistance ΔP of the cooling air circulation system. Generally, ΔP_f = (1.5~2) ΔP. The resistance ΔP of the cooling air circulation system can be calculated by the Formula (21):

$$\Delta P = \Delta P_R + \Delta P_I \tag{21}$$

In the formula, ΔP is the cooling air circulation resistance, Pa; ΔP_R is the cooling air flow resistance through the radiator, Pa; ΔP_I is the resistance other than the cooling air flow through the radiator. Generally, ΔP_I = (0.4~1.1) $\Delta \mathrm{P_R}$.

2.4. Water Characteristics Model

2.4.1. Radiator Water Resistance Model

Radiator cooling water resistance refers to the energy loss caused by the acceleration, rotation and eddy current of the coolant when the coolant flows in the radiator pipeline. The internal water side resistance of the radiator can be calculated by the Formula (22):

$$\Delta P_w = \frac{\rho_w u_w^2}{2}(4fi \cdot l/D_w + \xi)I_l \tag{22}$$

In the formula, ρ_w is the cooling water density in the radiator, kg/m^3; u_w is the cooling water flow rate in the radiator pipe, m/s; f_i is the friction factor; l is the length of the cooling water pipe in the radiator, m; D_w is the radiator diameter of inner cooling water pipe, m; ξ is the local resistance coefficient inside the radiator; I_l is the number of cooling water pipes in the radiator.

2.4.2. Electric Water Pump Model

The electric water pump is an important component of the car MCCS. The pump model needs to provide the flow rate of the pump at a certain speed and also needs to provide the flow rate when the external pressure is 0. The performance curve of the electric water pump can be described by the Formula (23):

$$\begin{cases} V_{H_2O} = V_0 - a(\Delta p)^b a = \frac{V_\mathrm{r}}{(\Delta p)_o^b - (\Delta p)_r^b} \\ V_0 = \mathrm{V_r} \times \frac{1}{1-[(\Delta p)_r/(\Delta p)_0]^b} \\ a = \frac{V_\mathrm{r}}{(\Delta p)_o^b - (\Delta p)_r^b} \end{cases} \tag{23}$$

The pressure rise rate and flow rate are calculated by the Formula (24):

$$\begin{cases} \Delta p = (\Delta p)_0 \left[1 - \frac{V}{V_0}\left[((\Delta p)_r/(\Delta p)_0\right]^b\right]^{1/b} \\ V = V_r \cdot \frac{1-[(\Delta p)/(\Delta p)_0]^b}{1-[(\Delta p)_r/(\Delta p)_0]^b} \end{cases} \tag{24}$$

In the formula, Δp is the pressure increase rate of the cooling water pump, Pa; V_0 is the maximum volume flow rate of the cooling water pump, m^3/s; b is the pressure rise index of the cooling water pump; V_r is the reference volume flow rate of the cooling water pump, m^3/s; $(\Delta p)_r$ is the reference cooling water pump pressure rise rate, Pa; $(\Delta p)_0$ is the cooling water pump pressure rise rate when the external pressure is 0, Pa.

2.5. Thermal Performance Simulation

2.5.1. Three-Dimensional Flow Field Simulation

There are many components in the front cabin of a car, and these components are placed very compactly. This makes the cabin structure complex, and it is easy to block the cooling air flow, causing local backflow and heat damage. Therefore, the analysis of the flow field and temperature field in the front cabin is a point that needs to be paid attention to in the field of heat balance. In the following, the velocity field and temperature field distribution in the Y and Z directions are intercepted after the simulation, and then the distribution characteristics of the flow field and temperature field in the front cabin are studied. After the flow field simulation, the average air inlet wind speed on the surface of each core body under the idling charging condition is obtained, as shown in Table 1. According to the characteristics of idling charging conditions, the rotating suction of each cooling fan is the main driving force for the incoming air to flow into the front cabin. After the cooling air enters the front cabin, it cools the high-temperature components in the cabin and takes away part of the heat.

Table 1. Average inlet air speed on the surface of each core.

Part	Surface Average Wind Speed
Condenser	6.08 m/s
Main radiator	5.76 m/s
Left auxiliary radiator	4.15 m/s
Right auxiliary radiator	4.54 m/s

As shown in Figure 2, it can be observed from the front cabin velocity field section of Y = 0 that the cooling air passes through the radiator, the suction effect of the cooling fan is not very significant, and there is an obvious vortex at the end of the back of the cooling fan. The heat accumulated around the PEMFC cannot be discharged in time, resulting in the accumulation of heat and excessive temperature. In addition, part of the cooling air flows into the upper space of the front cabin; it can be found that the baffles on the upper part of the front cabin block the cooling air and form a backflow, and the corresponding areas where the relative air does not circulate will also be relatively high.

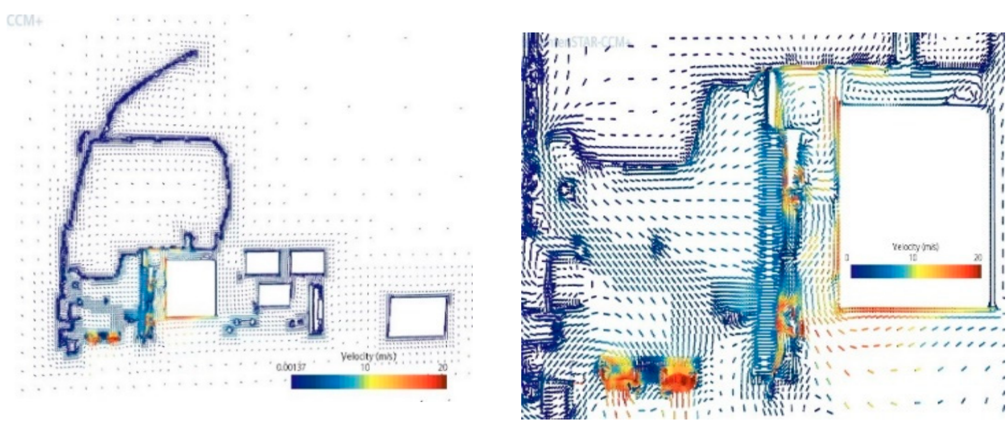

(**a**) (**b**)

Figure 2. Cross section of velocity field front cabin with Y = 0: (**a**) Overall Sectional View; (**b**) Partial Sectional View.

2.5.2. One-Dimensional Flow Field Simulation

According to the model built above, the water resistance and heat dissipation simulation of the MCCS is performed. The total water resistance in the final circuit is 35.50 kPa, and the total flow rate is 203.98 L/min. Among them, the flow rate in the main radiator circuit is 69.85 L/min, and the water resistance is 28.3 kPa; the flow rate in the left auxiliary radiator circuit is 61.49 L/min, and the water resistance is 32.62 kPa; and the flow rate in the right auxiliary radiator circuit is 72.64 L/min, and the water resistance is 34.50 kPa.

Figure 3 shows the heat dissipation simulation results of the FCV MCCS. The temperature difference between the inlet and outlet of the PEMFC coolant is about 12.9 °C, which proves that the designed system has a good cooling effect. The outlet temperature of the coolant is 78.7 °C, which meets the requirement of the outlet water temperature of the PEMFC in the MCCS. The temperature simulation results of the main and auxiliary radiators are shown in Table 2:

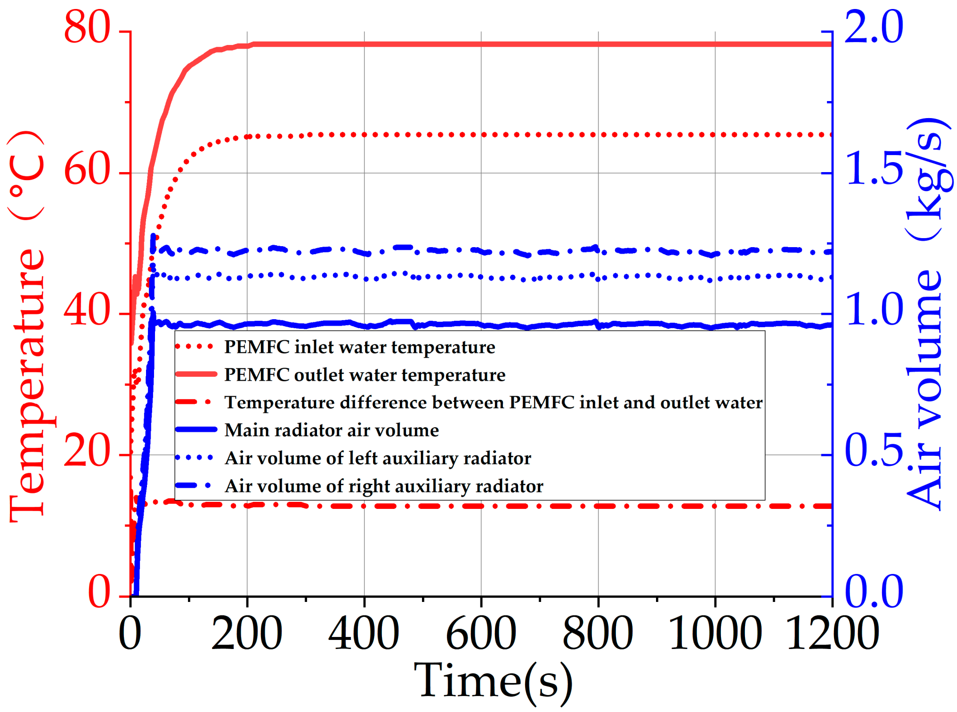

Figure 3. PEMFC thermal performance simulation results of MCCS.

Table 2. Temperature simulation results of main and auxiliary radiators.

Part	Air Volume	Inlet Water Temperature	Outlet Water Temperature	Outlet Air Temperature
Main radiator	0.96 kg/s	78.54 °C	64.10 °C	61.74 °C
Left auxiliary radiator	1.13 kg/s	78.54 °C	65.72 °C	63.82 °C
Right auxiliary radiator	1.22 kg/s	78.54 °C	66.84 °C	63.73 °C

According to the simulation results, the designed water pump can meet the total resistance requirement of the system (70 kPa), and the water resistance and flow rate of the main and auxiliary radiators are all at reasonable values. When the PEMFC is output at the highest power, the temperature of the water entering and exiting the PEMFC and the temperature of the water entering and exiting the main and auxiliary radiators are all at reasonable values.

3. Thermal Performance Optimization

3.1. Sensitivity Analysis

3.1.1. Main and Auxiliary Cooling Circuit Flow Distribution

The present study aims: carry out sensitivity analysis on the coolant flow rate of the main and auxiliary radiators in the MCCS, calculate the sensitivity coefficient according to the basic value of the input data and the common fluctuation range above and below the basic value, and verify the impact of the coolant flow rate of the main and auxiliary radiators on the cooling performance of the MCCS. The sensitivity analysis results of the radiator coolant flow in the MCCS are shown in Table 3:

Table 3. Sensitivity analysis results of coolant flow in main radiator.

Part	Radiator Coolant Flow Increment 100%	Water Temperature Decrement 100%	Absolute Value of Water Temperature Decrease	Sensitivity Value
Main radiator	0%	0.00%	0	0
	10%	0.48%	0.31	3.10
	20%	1.15%	0.74	3.70
	30%	1.71%	1.16	3.87
Auxiliary radiator	0%	0.00%	0	0
	10%	0.43%	0.28	2.80
	20%	0.85%	0.57	2.85
	30%	1.38%	0.91	3.03

3.1.2. Distance between Radiator and Fan

During the simulation analysis of the flow field in the front cabin, the factors that affect the air flow organization and heat dissipation in the cabin can be found; these are often attributed to the structure and layout. Table 4 shows the sensitivity analysis results for the optimization of the distance between the radiator and the cooling fan in the MCCS:

Table 4. Sensitivity analysis results of the distance between radiator and fan.

100% Increase in Distance between Radiator and Fan	100% Reduction in Water Temperature	Absolute Value of Water Temperature Drop	Sensitivity Value
0%	0.00%	0	0
10%	1.34%	0.86	8.60
20%	2.35%	1.51	7.55
30%	3.34%	2.14	7.13

When studying the influence of the distance between the radiator and the fan on the flow field in the front cabin, the distance between the fan and the radiator is continuously increased: the fan is moved away from the radiator in 10 mm, 20 mm, 30 mm and 40 mm increments, and the distance between other components is maintained. The position remains unchanged, and the three-dimensional simulation analysis of the flow field in the front cabin under the idling charging condition is carried out. Table 5 shows the results of the influence of the four layout schemes on the heat dissipation of the front cabin:

Table 5. Simulation results of each radiator and fan at each spacing.

Increase Distance between Radiator and Fan (mm)	Air Intake of Main Radiator (kg/s)	Air Intake of Left Auxiliary Radiator (kg/s)	Air Intake of Right Auxiliary Radiator (kg/s)	Total Air Intake of Fan (kg/s)	Air Intake of Radiator Increases Total Specific Gravity
0	0.960	1.130	1.220	0.813	0
10	0.968	1.136	1.224	0.832	1.890%
20	0.974	1.142	1.235	0.843	3.749%
30	0.981	1.154	1.241	0.846	6.032%
40	0.976	1.149	1.238	0.851	4.825%

Under the idling charging condition, when the distance between the radiator and the fan increases by 0 mm~30 mm, the air intake of each radiator shows a rising trend. Because the radiator fan is three-dimensionally twisted, when the fan rotates, part of the air flow cannot form an effective pressure difference. Therefore, a reasonable increase in the distance between the fan and the radiator can effectively increase the air intake speed on the surface of the main radiator core. When the distance is further increased, the air intake of each radiator is reduced. This is because the distance between the fan and the radiator is too large, which leads to the disorder of the flow field in the local area and the problem of blockage. Therefore, the distance between each radiator and fan is increased by 30mm at most.

3.2. Thermal Performance Optimization Model

Because there are many uncertain factors in the actual design of the front cabin MCCS that will eventually affect the thermal performance of the MCCS, the reliability of the uncertain factors is analyzed by the Taguchi Method. The purpose of the Taguchi Method design is to select a parameter combination that makes the experimental results stable and less volatile, and, based on a small number of experiments, the optimization trend is obtained. In order to make the selection of the MCCS experimental data more reasonable, the L8 orthogonal table is used to select experimental parameters, arrange experiments and evaluate more factors that affect the experimental results through fewer parameter combinations. The factors affecting the experimental results of the static Taguchi Method experiment in this paper can be divided into six controllable factors (parameters) and noise factors (random errors). By adjusting the level of controllable factors (parameters), the influence of noise on experimental results can be reduced. The signal-to-noise ratio was used to evaluate the stability of the experimental results, and the optimal level (parameter value) of each factor was selected according to the PEMFC effluent temperature response characteristics. Using the Taguchi Method can improve the quality of the MCCS, free engineers from trial and error and improve design efficiency. The experiment steps are as follows: build a mathematical model according to the structural characteristics of each component of the MCCS, establish the objective of the reliability cooling system design function, determine each influencing test factor and level number, establish a reasonable orthogonal test table and formulate a test plan. The Taguchi Method designs the reliability of the front cabin MCCS into the simulation verification process and resists the interference of uncontrollable factors by controlling the design scheme of the source. In the Taguchi Method, the signal-to-noise ratio η is a reliability index of MCCS thermal performance, mainly including the following:

(1) The signal-to-noise ratio of the target value., That is, the optimal target is m, and the system output characteristics are y_1, y_2, y_3,..., y_n; a total of n output characteristic values, according to the optimal target and output characteristics are as follows (25). To calculate the signal-to-noise ratio η:

$$\begin{cases} \eta = \frac{S_m - V_e}{nV_e} \\ V_e = \frac{\sum\limits_{i=1}^{n} (y_t - \overline{y})^2}{n-1} \\ S_m = \frac{\left(\sum\limits_{i=1}^{n} y_t\right)^2}{n} \end{cases} \tag{25}$$

(2) Look at the signal-to-noise ratio of small features. That is, the smaller the output response value, the better. Generally, noise, error and wear of parts are considered. The signal-to-noise ratio of the small feature can be calculated by the following Formula (26):

$$\eta = \frac{n}{\sum\limits_{i=1}^{n} y_t^2} \tag{26}$$

(3) Look at the signal-to-noise ratio of the characteristics. That is, the larger the output response value, the better. Generally, the coolant flow rate, cooling fan air volume and wear amount are considered. The signal-to-noise ratio of the small feature can be calculated by the following Formula (27):

$$\eta = \frac{\sum\limits_{i=1}^{n} y_t^2}{n} \tag{27}$$

(4) Signal-to-noise ratio of dynamic characteristics. Taking the output target value as an example, determine the relationship between MCCS thermal performance reliability and SN

ratio. If the output characteristic of the MCCS is the target value y, which obeys the normal distribution N (m, σ^2), m is the target value, and the cooling performance limit is set to Δ_0; that is, when $|y - m| < \Delta_0$, the specified cooling requirements can be completed. Otherwise, the MCCS does not meet the standard, and the performance reliability currently is:

$$R = P\{m - \Delta_0 < y < m + \Delta_0\} \tag{28}$$

Substitute $\sigma = \Delta_0/k$ into the Formula (29) to get:

$$R = P\{m - k\sigma < y < m + k\sigma\} = 2\phi(k) - 1 \tag{29}$$

At this time, the SN ratio is shown in the following Formula (30):

$$\eta = \frac{m^2}{\sigma^2} = \frac{k^2 m^2}{\Delta_0^2} \tag{30}$$

Substitute k = 1, 2, 3, 4 into the above formula, as shown in Table 6.

Table 6. Relationship between reliability and signal-to-noise ratio.

K	**1**	**2**	**3**	**4**
R	0.6724	0.9617	0.9943	0.999937
η	η_1	$4\eta_1$	$9\eta_1$	$16\eta_1$

It can be seen from the above table that the greater the SN ratio of the thermal performance output by the MCCS, the greater the reliability of the MCCS. Similarly, the above-mentioned characteristics are not only suitable for quickly obtaining the target value but also suitable for the minimum, maximum and dynamic characteristics. Through the above analysis and comparison, it can be concluded that the reliability design of the signal-to-noise ratio in the Taguchi Method is roughly the same as the reliability design of the thermal performance of the MCCS.

3.3. Thermal Performance Optimization Design

Under the MCCS designed for this model, the outlet water temperature of the PEMFC is 78.7 °C. Since the optimization goal in this paper is to reduce the outlet water temperature of the PEMFC, the optimization system characteristic is a small characteristic problem. The actual engineering and simulation experience recommends the selection of six design parameters that, among all the factors affecting the thermal performance of MCCS, have the greatest impact. These six design parameters are the main and auxiliary radiator air intake speed, the main and auxiliary radiator core area, water pump speed ratio and heating pipe diameter. By adjusting these six design parameters, we hope to solve the current quality problems. These design parameters that must be systematically changed during the experiment are called "controllable factors" and use the English letters A, B, C, . . . , etc. to represent the control factor. Each factor is set to two levels, and the noise factor only considers the ambient temperature of 38 °C. Among them, the air intake speed of the main and auxiliary radiators, the core area of the main and auxiliary radiators and the pipe diameter can all be realized by changing the parts. Although the change of pump speed ratio is a controllable factor, it should be taken as a follow-up alternative measure. The purpose of the experiment is to determine the set values of the controllable factors. Controllable factors and levels are shown in Table 7.

The experiment then requires selection of the appropriate orthogonal table according to the controllable factors in MCCS and the values of each level in the table above. The selection principle of the orthogonal table is that under the premise that the experimental factors and interactions can be arranged, the smaller orthogonal table should be selected as much as possible to reduce the number of experiments. In general, the number of levels of test factors should be equal to the number of levels in the orthogonal table; the number of factors (including interaction) should not be greater than the number of columns in the orthogonal table; and the sum of the degrees of freedom of each factor and interaction should be less than the specified. Next, the total degrees of freedom of the orthogonal table is chosen, in order to estimate the experimental error. Since the number of levels in each column is 2, an equal-level orthogonal table is used. In this example, there are six 2-level factors, and L8 (2^7) or L12 (2^{11}) can be selected. However, this test only examines the effects of the six factors on the PEMFC outlet water temperature. Influence effect does not examine the interaction between factors, so it is better to choose L8 (2^7) orthogonal table. To examine the interaction, L12 (2^{11}) should be used. Eight combination schemes are determined in the test table. Compared with the full factor test combination of 2^6 = 64 tests, the number of orthogonal optimization tests is reduced by 87.5%. Using the one-dimensional simulation optimization model, the signal-to-noise ratio and PEMFC outlet water temperature of each combination scheme are obtained, as shown in Table 8.

Table 7. Controllable factors and levels table.

Project	A Main Radiator Air Intake Speed	B Auxiliary Radiator Air Intake Speed	C Main Radiator Core Area	D Auxiliary Radiator Core Area	E Water Pump Speed Ratio	F Heating Pipe Diameter
Level 1	6.00 m/s	4.60 m/s	0.52 m^2	0.43 m^2	1.35	15.8 mm
Level 2	6.25 m/s	4.75 m/s	0.58 m^2	0.46 m^2	1.52	12.0 mm

Table 8. Test combination scheme and simulation result table.

Controllable Factor	Ai	Bi	Ci	Di	Ei	Fi	Water Temperature/°C	S/N
Plan 1	1	1	1	1	1	1	77.35	−37.77
Plan 2	1	1	1	2	2	2	76.45	−37.67
Plan 3	1	2	2	1	1	2	75.00	−37.50
Plan 4	1	2	2	2	2	1	76.62	−37.69
Plan 5	2	1	2	1	2	1	77.91	−37.83
Plan 6	2	1	2	2	1	2	78.76	−37.93
Plan 7	2	2	1	1	2	2	75.32	−37.54
Plan 8	2	2	1	2	1	1	78.87	−37.94

Based on the combination scheme in the above table, the PEMFC outlet water temperature response analysis diagram and the signal-to-noise ratio response analysis diagram are drawn, as shown in Figure 4.

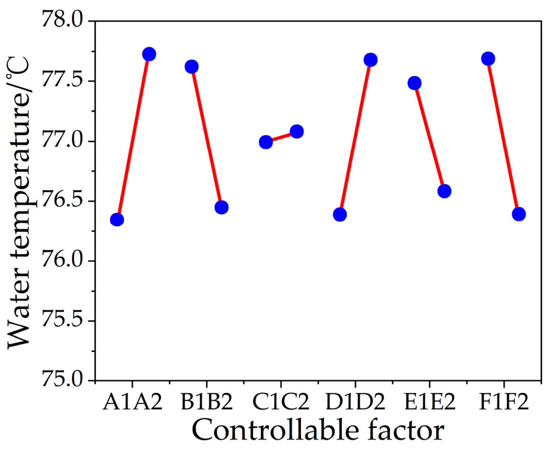

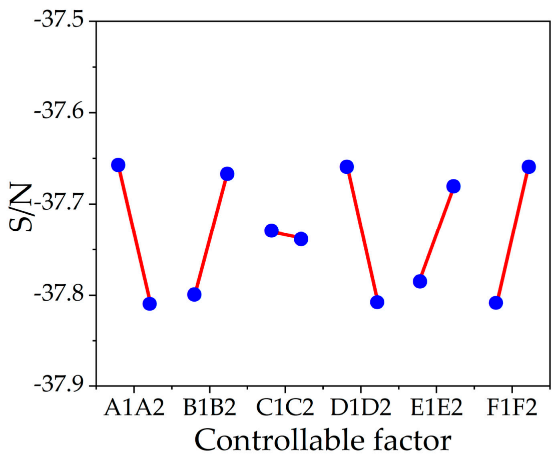

Figure 4. (**a**) Analysis of temperature response of reactor effluent; (**b**) S/N response analysis.

Measured values of quality characteristics are not suitable for direct use as quality indicators. In the Taguchi Method, the S/N ratio is used as the unit of measurement for the thermal performance of the MCCS. According to the characteristics of the corresponding variables, the signal-to-noise ratio with the smallest characteristics is selected; that is, the smaller the output response value, the better. The factor effect refers to the influence of the change of the control factor on the S/N ratio or quality characteristics. When the change of a factor will have a significant impact on the S/N ratio (or quality characteristics), the factor is called an important factor. It can be seen from the response analysis diagram that controllable factor A, controllable factor D and controllable factor F are important factors affecting the final PEMFC outlet water temperature and are also factors that have the greatest impact on reliability. From the data in the above table, we can see that the effects of the three effects are almost the same. The factor effect is large, and it is an important factor The controllable factors B and E have a certain influence on the outlet water temperature of the PEMFC and are regarded as adjustment factors; the controllable factor C has little effect on the robustness and is regarded as a secondary factor. So, A2/B2/C1/D2/E2/F2 is chosen as the initial optimal combination. However, changing D, E and F at the same time in actual engineering practice will result in a substantial increase in the cost of transformation. Considering factors such as the cost and time required for optimization, it is decided to choose A2/B2/C1/D2/E2/F2 and A2/B1/C1/D2/E1/F1, which are compared and analyzed. Table 9 shows the comparison of the results of the two optimization schemes in the one-dimensional simulation.

Table 9. Optimization scheme combination and simulation results comparison.

Controllable Factors	Ai	Bi	Ci	Di	Ei	Fi	Water Temperature/°C
Plan 9	2	2	1	2	2	2	74.26
Plan 10	2	1	1	2	1	1	74.63

Among them, Plan 9 is the combination of A2/B2/C1/D2/E2/F2, and Plan 10 is the combination of A2/B1/C1/D2/E1/F1. The outlet water temperature of the PEMFC is 74.26 °C in Plan 9. However, the optimization of the water pump speed ratio F not only affects the service life of the system components, but also increases the cost and time of the transformation, so it is decided to ignore the impact of the change of the water pump speed ratio. The outlet water temperature of the PEMFC is 74.63 °C in Plan 10, which is only 0.37 °C higher than the target outlet water temperature of the PEMFC in Plan 9 for the cooling system design. Considering the reasons such as the design margin and the error caused by the simulation, as well as the cost of structural optimization and the optimization time, etc., it is determined that Plan 10—that is, the combination of schemes A2/B1/C1/D2/E1/F1—is the best optimization scheme; compared with the original scheme, this scheme just optimizes the core area of the auxiliary radiator and the air intake speed of the main radiator, and the cost and duration of optimization are relatively low, which are in line with the actual engineering indicators.

3.4. Thermal Performance Optimization Results

Substituting the optimized best parameter combination into the three-dimensional simulation, under the idling charging condition, the improvement phenomenon of the formulated improvement plan is more obvious, so the flow field nephogram under the idling charging condition is intercepted for analysis. It can be seen from Figure 5 that the cooling air is divided into two parts after entering from the left air intake grille, and a small part of the gas is sucked into the condenser for heat exchange. After optimization, the gas circulation is obviously smoother, and the gas flow rate is larger.

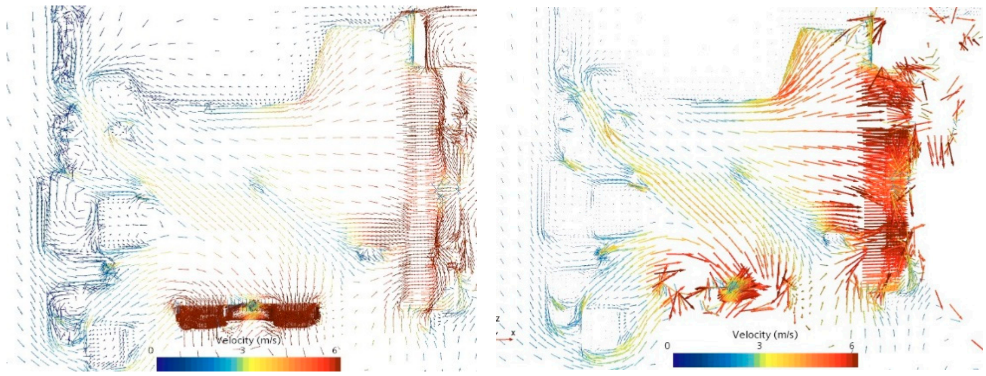

(**a**) (**b**)

Figure 5. Simulation diagram of cooling air flow after entering the grille: (**a**) before optimization; (**b**) after optimization.

However, as shown in Figure 6, most of the gas is inhaled by the main radiator; the air flow in some areas around the main radiator is no longer disorderly compared with before optimization, and there is no backflow phenomenon. It can smoothly enter the front cabin to quickly cool down the high-temperature components, the heat is taken away, the proportion of the air intake of the main radiator is significantly increased and the cooling performance is also improved.

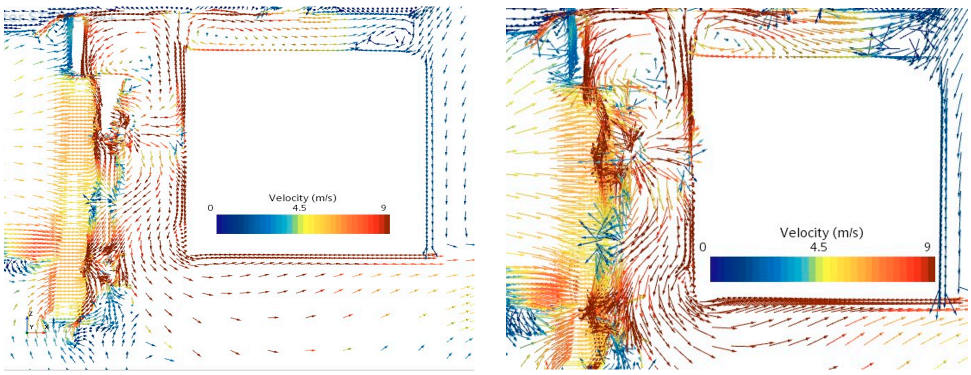

(**a**) (**b**)

Figure 6. Flow field around the main radiator under vehicle simulation: (**a**) before optimization; (**b**) after optimization.

As shown in Figure 7, in the environment that keeps the temperature constant and ensures the water flow rate of the PEMFC, the cooling system mainly improves the heat dissipation effect by improving the heat transfer performance of each radiator core and the wind speed of the radiator cooling fan. Therefore, when optimizing the outlet water temperature of the PEMFC, the core area of the auxiliary radiator is mainly adjusted, and then the air intake through the radiator is adjusted. The air intake of the optimized auxiliary radiator is significantly improved, the air volume distribution is more uniform and the wind speed is more stable. The heat dissipation effect is more obvious.

After the simulation of the three-dimensional model of the MCCS is completed, the air volume results of each radiator are substituted into the one-dimensional simulation model for water resistance and water temperature simulation. The flow rate is stable at 200.07 L/min, and the total water resistance is stable at 36.14 kPa; the flow rate in the main radiator circuit is 72.36 L/min, and the water resistance is 28.32 kPa; the flow rate in the left auxiliary radiator circuit is 63.58 L/min, and the water resistance is 32.62 kPa; the flow rate in the right auxiliary radiator circuit is 64.13 L/min, the water resistance is 33.72 kPa, the optimized water resistance and flow data are shown in Table 10, and the temperature difference between the inlet and outlet of the PEMFC coolant is about 13.4 °C, which proves that the designed MCCS has a good cooling effect. The outlet temperature of the coolant is 75.8 °C. Based on meeting the temperature requirements of the PEMFC outlet water in the MCCS, the heat dissipation effect is significantly improved compared with the original solution.

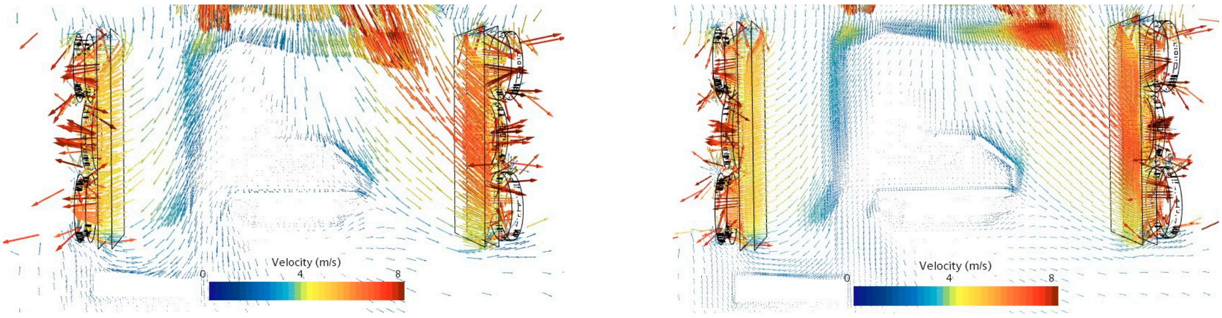

(**a**) (**b**)

Figure 7. Flow field around two auxiliary radiators under vehicle simulation: (**a**) before optimization; (**b**) after optimization.

Table 10. Optimized water resistance and flow data.

Loop	Flow	Water Resistance
Total circuit	200.07 L/min	36.14 kPa
Main radiator circuit	72.36 L/min	28.32 kPa
Left auxiliary radiator circuit	63.58 L/min	32.62 kPa
Right auxiliary radiator circuit	64.13 L/min	33.72 kPa

Table 11 shows the one-dimensional simulation results of the main and auxiliary radiators. According to the simulation results, the optimization scheme can meet the total resistance requirement of the system (70 kPa) based on the original, and the water resistance and flow of the main and auxiliary radiators are equal. Compared with the original scheme, when the PEMFC outputs are 117 kW, the inlet and outlet water temperatures of the PEMFC and the inlet and outlet water temperatures of the main and auxiliary radiators are lower, which further proves that this optimization scheme is more effective.

Table 11. Simulation results of each radiator after optimization.

Part	Air Volume	Water Temperature	Water Temperature	Outlet Temperature
Main radiator	1.26 kg/s	74.26 °C	62.37 °C	60.83 °C
Left auxiliary radiator	1.57 kg/s	74.26 °C	63.54 °C	61.94 °C
Right auxiliary radiator	1.62 kg/s	74.26 °C	64.19 °C	62.35 °C

4. Thermal Performance Optimization Experimental Vehicle Verification

4.1. Experimental Objects

This experiment is based on the experiment of the MCCS. The PEMFC experimental vehicle used in this experiment is a light truck independently developed by a certain company. The vehicle is a hydrogen PEMFC hybrid box-type truck with a body length of 9 m, a height of 3 m, a width of 2.4 m, and a wheelbase of 5.8 m. The rated power is 117 kw, the total mass of the vehicle is 10,530 kg, and the temperature of the PEMFC coolant is not higher than 85 °C. The photos of the vehicle are shown in Figure 8.

Figure 8. Experimental vehicle.

4.2. Experimental Equipment

Experimental instruments and equipment should be calibrated before use, used within the validity period, and adjusted to ensure normal operation and accurate load requirements. The required experimental equipment includes a fault diagnosis instrument, flow meter, temperature sensor, anemometer, data acquisition card, vehicle-mounted inverter, etc. During the experiment, in order to facilitate the evaluation of the cooling effect of each radiator, the detection points of each sensor were selected as follows: T1: water inlet temperature of the main radiator; T2: water inlet temperature of the left auxiliary radiator; T3: water inlet temperature of the right auxiliary radiator; T4: water outlet flow rate of main radiator; T5: water outlet flow rate of left auxiliary radiator; T6: water outlet flow rate of right auxiliary radiator; T7: water outlet temperature of main radiator; T8: water outlet temperature of left auxiliary radiator; T9: Water outlet temperature of the right auxiliary radiator; T10: PEMFC inlet water temperature; T11: PEMFC outlet water temperature. Typical sensor installation positions are shown in Figure 9:

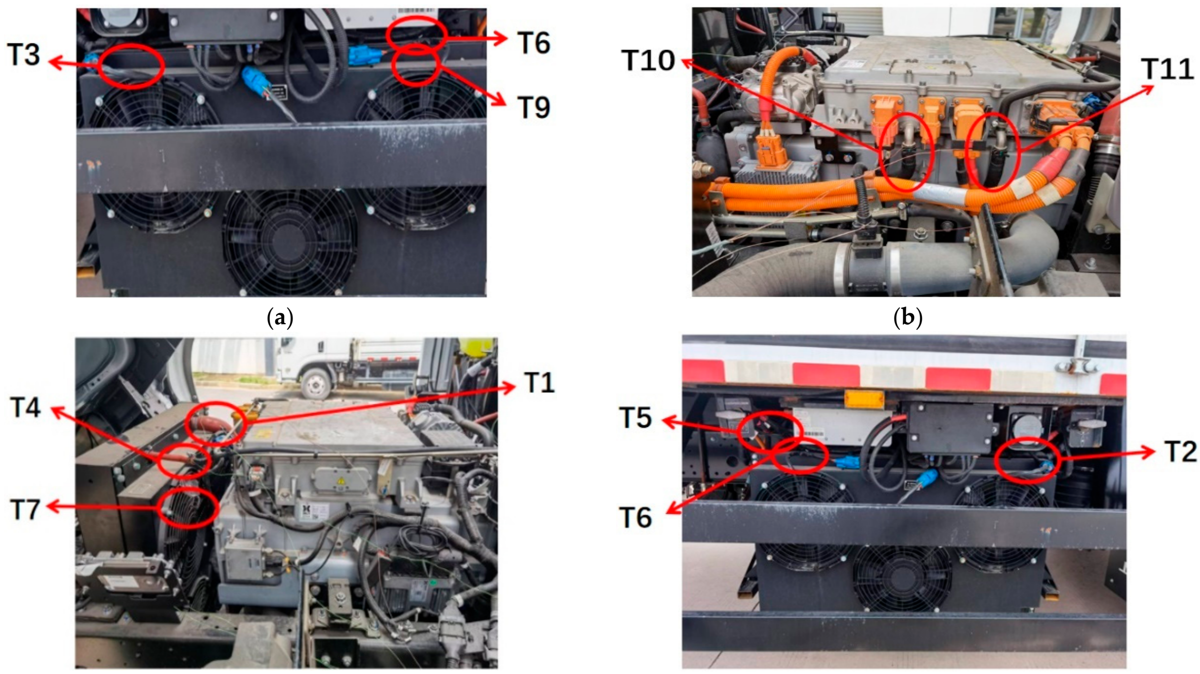

(**a**) (**b**) (**c**) (**d**)

Figure 9. Experimental sensor arrangement: (**a**) right auxiliary radiator sensor arrangement; (**b**) PEMFC sensor arrangement; (**c**) main radiator sensor arrangement; (**d**) left auxiliary radiator sensor arrangement.

4.3. Experimental Method

To ensure the integrity and reliability of the experiment, the experiment was tested in the following four working conditions: (1) Full power idling charging condition; (2) Half power idling charging condition; (3) Constant speed of 40 km/h working condition; (4) Constant speed of 80 km/h working condition. This experiment verifies the heat balance of the whole vehicle on the outdoor road, so the outdoor road of the experiment is required to be free from rain and fog, the wind speed should not exceed 3 m/s and the ambient temperature should not be lower than 30 °C. Due to the influence of heat accumulation near the PEMFC, ground radiation, hot air backflow and other factors, as the ambient temperature rises, the temperature of the PEMFC and coolant will rise faster than the ambient temperature. In other words, the experiment will get a higher allowable ambient temperature experimental result at a lower ambient temperature, and the actual effect can only be obtained when the ambient temperature is close to the target ambient temperature. Therefore, the ambient temperature cannot be lower than 30 °C. For the road itself, the road surface is required to be hard, smooth, clean, dry and paved with concrete or asphalt. The experimental vehicle itself should be maintained according to the vehicle technical conditions or instructions to keep the experimental vehicle in good technical condition. The appearance should be symmetrical, and the body should be upright; the free pedal stroke of the clutch should be correct; the opening of the accelerator pedal should be checked; the vehicle should not be adjusted, replaced, maintained or repaired during the experiment.

The experimental steps are as follows: (1) Adjust and maintain the experimental prototype vehicle, and check whether the vehicle is powered on; (2) Install the temperature sensor and flow meter correctly to ensure that the connection is tight; (3) Warm up and drive, by observing the PEMFC water temperature. Determine whether the experimental prototype vehicle has completed the warm-up driving; (4) Check whether the data collector is powered on and whether the upper computer is charging, to prevent the interruption of data acquisition and storage; (5)When each cooling medium reaches thermal equilibrium within 8 min, the experimental condition ends; (6) After the experiment, each test sensor is disassembled, and the collected data is processed and analyzed.

4.4. Experimental Results

A real vehicle was tested at a test site for full power idling charging, half power idling charging, and heat balance experiments at a constant speed of 40 km/h and a constant speed of 80 km/h. The ambient temperature of the test site was about 38 °C, the humidity was 26% and the wind speed 1.9 m/s. Through the experiment of each sensor arranged, as shown in the previous section, the experimental data and results under this working condition are shown in Table 12.

4.4.1. Idling Charging Condition

As shown in Figure 10a, the temperature of the experimental site is 38 °C, and the temperature of the PEMFC outlet water changes within 12 min under the condition of full-power idling charging of the whole vehicle. The liquid-air temperature difference has been controlled within 55 °C, which meets the heat dissipation requirements. Comparing the outlet water temperature, the curve of this experiment with the PEMFC outlet water temperature and the curve of the previous simulation, when the experimental value and the simulation value are stable, the PEMFC outlet water temperature is relatively similar, which proves that the previous simulation is correct and referable. Under the same experimental conditions, the actual water outlet temperature of the main and auxiliary radiators is higher than that of the simulation, but the error is within the allowable range. About 12 min after the main and auxiliary radiators are turned on, the outlet water temperature does not change. The cooling system has reached a state of thermal equilibrium, the outlet water temperature of the main and auxiliary radiators is less than 70 °C and the liquid-air temperature difference is within 50 °C. Under this working condition, the heat dissipation performance of the cooling system can smoothly meet the heat dissipation requirements.

Table 12. Experimental data and results.

Vehicle Condition	Full Power Idle Charging	Half Power Idle Charging	Uniform Speed 40 km/h	Uniform Speed 80 km/h
Main radiator coolant flow rate (L/min)	74.21	73.96	73.45	73.84
Left auxiliary radiator flow rate (L/min)	64.15	65.28	65.71	65.41
Right auxiliary radiator flow rate (L/min)	65.74	66.13	65.86	66.39
PEMFC inlet water temperature (°C)	66.23	64.46	64.63	62.05
PEMFC outlet water temperature (°C)	76.05	75.18	75.35	74.53
Ambient temperature of the vehicle (°C)	38	38	38	38
Liquid-air temperature difference of each radiator (°C)	50	50	50	50
Air intake grill wind speed in front cabin (m/s)	2.24	2.23	6.57	10.03
Outlet water temperature of main radiator (°C)	64.09	61.05	61.26	60.16
Outlet water temperature of left auxiliary radiator (°C)	65.03	62.04	61.65	61.52
Outlet water temperature of right auxiliary radiator (°C)	65.65	62.84	63.25	61.55

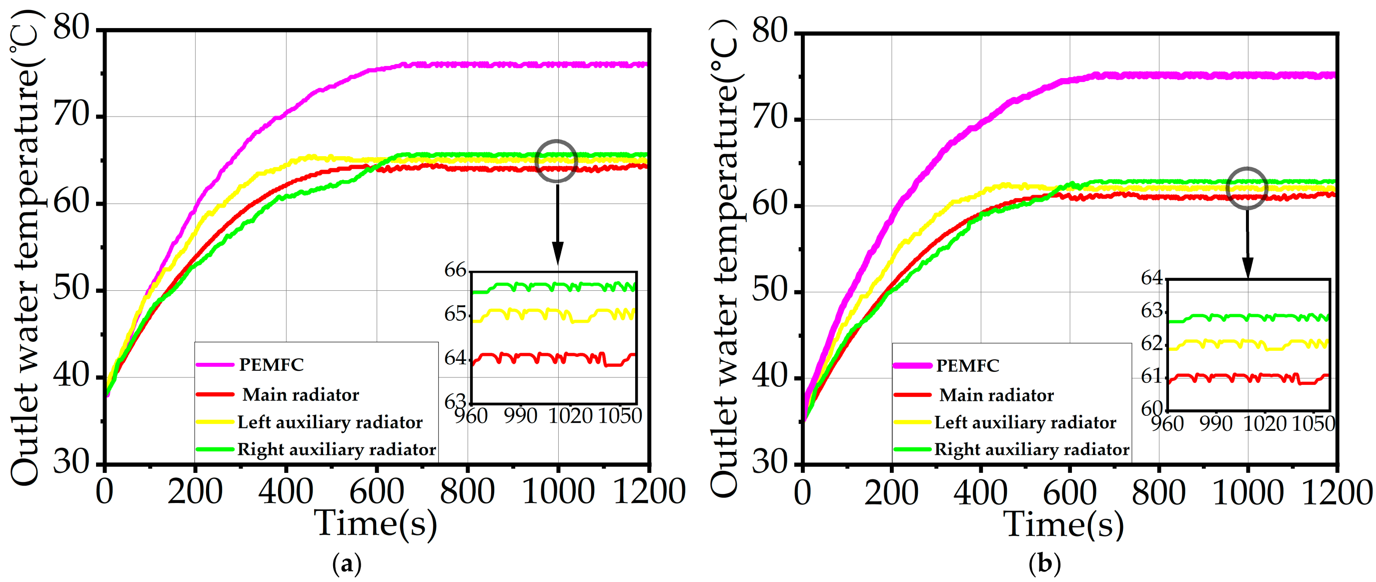

Figure 10. Outlet water temperature change curve: (**a**) Full power idling charging condition; (**b**) Half power idling charging condition.

The experimental data show that compared with full power idling charging, PEMFC heat generation is smaller under half power idling charging, and the temperature of the water entering and exiting each radiator is also lower because different extreme working conditions do not affect the distribution of coolant. Therefore, the flow rate of the main and auxiliary radiators is similar to that of the full power idling charging condition. Figure 10b shows the temperature change curve of the PEMFC outlet water under this working condition; it can also be seen that 12 min after the start of the experiment, the temperature of the PEMFC outlet water does not change anymore, and the whole vehicle reaches a thermal equilibrium state. The fan speeds of the main and auxiliary radiators are the same as those under the condition of full power idling charging. As shown in Figure 10b, it can also be seen that 12 min after the start of this working condition, the outlet water temperature of the main and auxiliary radiators is less than 70 °C; this shows that the MCCS has good heat dissipation performance.

4.4.2. Uniform Speed Condition

The experimental data show that when the real vehicle is running at a constant speed of 40 km/h, compared with the idling charging condition, the wind speed of the air intake grille in the front cabin is significantly increased, the air intake of the MCCS is increased and the outlet water temperature of each radiator is lowered, which helps improved cooling performance. Under this working condition, the outlet water temperature of the PEMFC, the outlet water temperature of each radiator and the flow rate of coolant all meet the heat dissipation requirements. The change curve is shown in Figure 11a. The temperature of the experimental site is 38 °C. After the vehicle runs a 9 km straight track at a constant speed of 40 km/h, there is basically no change in the PEMFC outlet water temperature after 12 min. The outlet water temperature of the PEMFC is less than 80 °C, and the liquid-air temperature difference has been controlled within 55 °C. Under this working condition, the outlet water temperature of the PEMFC can smoothly meet the heat dissipation requirements. As shown in Figure 11a, about 12 min after the main and auxiliary radiators are turned on, the outlet water temperature does not change any more, the MCCS reaches a thermal equilibrium state and the outlet water temperature of the main and auxiliary radiators is less than 70 °C. The liquid-air temperature difference is within 50 °C. Under this working condition, the heat dissipation performance of the MCCS can successfully meet the heat dissipation requirements.

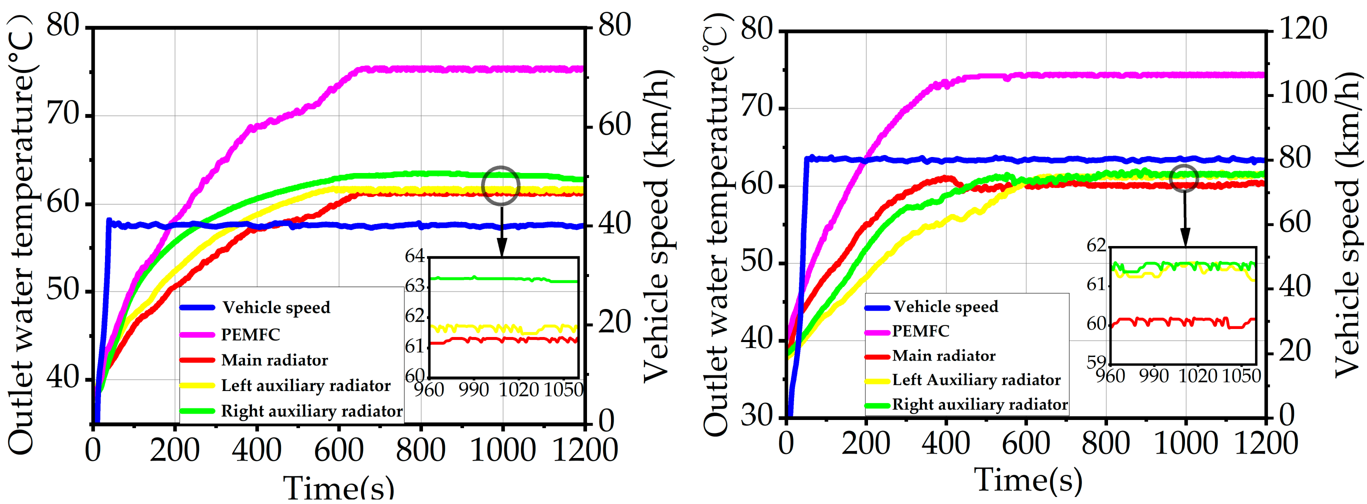

Figure 11. Outlet water temperature change curve: (**a**) Constant speed 40 km/h working condition; (**b**) Constant speed 80 km/h working condition.

The experimental data show that, compared with the working condition of 40 km/h at a constant speed, the heat generated by the PEMFC is larger under the working condition of a constant speed of 80 km/h, but the wind speed of the air intake grille in the front cabin will also be significantly increased, and the air intake of the MCCS will increase, so there will be more air volume per unit time to take away the heat generated by the PEMFC, and the temperature of the inlet and outlet water of each radiator will be lower, because different extreme working conditions will not affect the distribution of coolant; therefore, the flow rate of the device is similar to the working condition of a constant speed of 40 km/h. Figure 11b shows the change curve of the PEMFC outlet water temperature under this working condition: it can also be seen that 12 min after the start of the experiment, the PEMFC outlet water temperature does not change, and the whole vehicle reaches a thermal equilibrium state. The fan speeds of the main and auxiliary radiators are the same as those under the condition of constant speed of 40 km/h. As shown in Figure 11b, it can also be seen that 12 min after the start of this working condition, the temperature is less than 70 °C; this shows that the MCCS has good heat dissipation performance.

5. Conclusions

PEMFC have the advantages of high efficiency and environmental protection, and they are gradually replacing traditional engines as the power source of new energy vehicles. Unlike engine heat that is mainly dissipated by exhaust gas flow and cylinder block radiation, 95% of the heat generated by PEMFC electrochemical reactions needs to be taken away by cooling water. The development and optimization of FCV cooling systems has become one of the hot spots and difficulties today. In this paper, a FCV MCCS is taken as the research object, and the numerical simulation method is used to study the design and optimization performance of the vehicle's PEMFC MCCS, which can provide reference for the development and design of the vehicle's front compartment cooling system. The main research contents are as follows:

(1) Determine the structure and working principle of the PEMFC MCCS designed in this paper, classify the existing components according to the actual operation of the MCCS and establish a mathematical model for the coupling of heat, wind and water in the PEMFC cooling system.

(2) In order to verify the matching performance of each component of the MCCS, the flow field distribution information flowing through the surface of each radiator is extracted, the parameter model of the cooling system is established and the wind speed matrix of each radiator is imported into the software for joint simulation, to obtain the flow field of each radiator inlet and outlet temperature and flow resistance. To verify the simulation results, this paper conducts PEMFC front cabin heat balance experiments and obtains relevant experimental results. The comparison results show that one-dimensional/three-dimensional joint simulation can get more accurate simulation results than single simulation. Co-simulation can consider the efficiency and accuracy of simulation and can provide a reference for the design of similar FCV cooling systems.

(3) Establish the objective function of cooling system reliability design based on the Taguchi Method; combined with the fuzzy comprehensive evaluation method, choose the A2/B1/C1/D2/E1/F1 scheme, and, the final PEMFC outlet temperature of 75.8 °C was reduced by 2.9 °C compared to the unoptimized simulation result. The temperature difference between the inlet and outlet of the PEMFC coolant is about 13.4 °C. While the cooling performance is improved, the spatial layout of each cooling component can also be optimized.

(4) Under the condition of full power idling charging, the temperature of the PEMFC water is 76.05 °C. After optimization based on the Taguchi Method, the temperature of the PEMFC outlet water is 75.8 °C. The experiment predicts that due to the obvious increase of the wind speed of the air intake grille in the front cabin, and the increase of the air intake of the MCCS, the outlet water temperature of the PEMFC is 75.35 °C under the condition of a constant speed of 40 km/h, and the outlet water temperature of the PEMFC is 74.53 °C under the condition of a constant speed of 80 km/h, which is lower than that under the idling charging condition. This verifies the rationality of the experimental results and confirms the reliability of the simulation results. The experimental results also show that about 12 min from the start of each working condition, the outlet water temperature of each outlet no longer fluctuates greatly, and the outlet temperature and flow rate are in line with the experimental expectations. The MCCS can indeed effectively solve the heat dissipation problem of the PEMFC and prove the effectiveness of the MCCS designed in this paper and the correctness of the one-dimensional/three-dimensional simulation.

Author Contributions: Conceptualization, H.H., H.D. and D.H.; methodology, H.H., H.D. and D.H.; formal analysis, H.H., H.D. and D.H.; investigation, H.H., Z.C. and C.Q.; resources, H.H. and D.H.; data curation, H.H., H.D., D.H. and C.Q.; writing—original draft preparation, H.H., H.D., D.H. and Z.C.; writing—review and editing, H.H., H.D. and D.H.; visualization, C.Q.; supervision, Y.S. and X.S.; project administration, Y.S. and X.S.; funding acquisition, Y.S. and X.S. All authors have read and agreed to the published version of the manuscript.

Funding: This research received no external funding.

Institutional Review Board Statement: Not applicable.

Informed Consent Statement: Not applicable.

Data Availability Statement: The data presented in this study are available on request from the corresponding author.

Conflicts of Interest: The authors declare no conflict of interest.

References

1. Yuan, Z.; Chuai, W.; Guo, Z.; Tu, Z.; Kong, F. Thermal Layout Analysis and Design of Direct Methanol Fuel Cells on PCB Based on Novel Particle Swarm Optimization. *Micromachines* **2019**, *10*, 641. [CrossRef] [PubMed]
2. Hu, D.; Liu, J.; Yi, F.; Yang, Q.; Zhou, J. Enhancing heat dissipation to improve efficiency of two-stage electric air compressor for fuel cell vehicle. *Energy Convers. Manag.* **2021**, *251*, 115007. [CrossRef]
3. Zhang, Y.; Zhang, C.; Huang, Z.; Xu, L.; Liu, Z.; Liu, M. Real-Time Energy Management Strategy for Fuel Cell Range Extender Vehicles Based on Nonlinear Control. *IEEE Trans. Transp. Electrif.* **2019**, *5*, 1294–1305. [CrossRef]
4. Cheng, S.; Hu, D.; Hao, D.; Yang, Q.; Wang, J.; Feng, L.; Li, J. Investigation and analysis of proton exchange membrane fuel cell dynamic response characteristics on hydrogen consumption of fuel cell vehicle. *Int. J. Hydrogen Energy* **2022**, *47*, 15845–15864. [CrossRef]
5. Li, M.; Bai, Y.; Zhang, C.; Song, Y.; Jiang, S.; Grouset, D.; Zhang, M. Review on the research of hydrogen storage system fast refueling in fuel cell vehicle. *Int. J. Hydrogen Energy* **2019**, *44*, 10677–10693. [CrossRef]
6. Hu, D.; Hou, W.; Hu, L.; Yang, L.; Yang, Q.; Zhou, J. Optimal operation region of super-high-speed electrical air compressor in fuel cell system for working stability under multiple-time scale excitation. *Int. J. Hydrogen Energy* **2021**, *46*, 20054–20064. [CrossRef]
7. Song, Y.; Zhang, C.; Ling, C.-Y.; Han, M.; Yong, R.-Y.; Sun, D.; Chen, J. Review on current research of materials, fabrication and application for bipolar plate in proton exchange membrane fuel cell. *Int. J. Hydrogen Energy* **2019**, *45*, 29832–29847. [CrossRef]
8. Hu, D.; Yang, L.; Yi, F.; Hu, L.; Yang, Q.; Zhou, J. Optimization of speed response of super-high-speed electric air compressor for hydrogen fuel cell vehicle considering the transient current. *Int. J. Hydrogen Energy* **2021**, *46*, 27183–27192. [CrossRef]
9. Li, Y.; Chang, G.; Zhao, W. Experimental Investigation on the Operating Characteristics of Flat-Plate CLPHP for PEMFC Cooling. *World Electr. Veh. J.* **2021**, *12*, 116. [CrossRef]
10. Rezk, H.; Fathy, A. Performance Improvement of PEM Fuel Cell Using Variable Step-Size Incremental Resistance MPPT Technique. *Sustainability* **2020**, *12*, 5601. [CrossRef]
11. Xiong, S.; Wu, Z.; Li, W.; Li, D.; Zhang, T.; Lan, Y.; Zhang, X.; Ye, S.; Peng, S.; Han, Z.; et al. Improvement of Temperature and Humidity Control of Proton Exchange Membrane Fuel Cells. *Sustainability* **2021**, *13*, 10578. [CrossRef]
12. He, T.; Shi, R.; Peng, J.; Zhuge, W.; Zhang, Y. Waste Heat Recovery of a PEMFC System by Using Organic Rankine Cycle. *Energies* **2016**, *9*, 267. [CrossRef]
13. Hu, D.; Wang, Y.; Li, J.; Yang, Q.; Wang, J. Investigation of optimal operating temperature for the PEMFC and its tracking control for energy saving in vehicle applications. *Energy Convers. Manag.* **2021**, *249*, 114842. [CrossRef]
14. Xu, J.; Zhang, C.; Fan, R.; Bao, H.; Wang, Y.; Huang, S.; Chin, C.S.; Li, C. Modelling and control of vehicle integrated thermal management system of PEM fuel cell vehicle. *Energy* **2020**, *199*, 117495. [CrossRef]
15. Zhang, Q.; Xu, L.; Li, J.; Ouyang, M. Performance prediction of proton exchange membrane fuel cell engine thermal management system using 1D and 3D integrating numerical simulation. *Int. J. Hydrog. Energy* **2018**, *43*, 1736–1748. [CrossRef]
16. Xing, L.; Xiang, W.; Zhu, R.; Tu, Z. Modeling and thermal management of proton exchange membrane fuel cell for fuel cell/battery hybrid automotive vehicle. *Int. J. Hydrogen Energy* **2021**, *47*, 1888–1900. [CrossRef]
17. Zhang, Q.; Tong, Z.; Tong, S.; Cheng, Z. Research on performance of liquid drive fan cooling system for hydrogen fuel cell forklift. *Int. J. Hydrogen Energy* **2022**, *47*, 9690–9705. [CrossRef]
18. Zhu, R.; Xing, L.; Tu, Z. Simulations and analysis of high-temperature proton exchange membrane fuel cell and its cooling system to power an automotive vehicle. *Energy Convers. Manag.* **2022**, *253*, 115182. [CrossRef]
19. Philip, N.; Ghosh, P.C. A generic sizing methodology for thermal management system in fuel cell vehicles using pinch analysis. *Energy Convers. Manag.* **2022**, *269*. [CrossRef]
20. Fly, A.; Thring, R. A comparison of evaporative and liquid cooling methods for fuel cell vehicles. *Int. J. Hydrogen Energy* **2016**, *41*, 14217–14229. [CrossRef]
21. Su, C.-Q.; Sun, J.-F.; Meng, G.-D.; Liu, X.; Wang, Y.-P. Thermal management control strategy of liquid-cooled fuel cell vehicle. *Energy Rep.* **2022**, *8*, 141–153. [CrossRef]
22. Kim, J.; Lee, S.-M.; Srinivasan, S.; Chamberlin, C.E. Modeling of Proton Exchange Membrane Fuel Cell Performance with an Empirical Equation. *J. Electrochem. Soc.* **1995**, *142*, 2670–2674. [CrossRef]
23. Amphlett, J.C.; Baumert, R.M.; Mann, R.F.; Peppley, B.A.; Roberge, P.R.; Harris, T.J. Performance Modeling of the Ballard Mark IV Solid Polymer Electrolyte Fuel Cell: I. Mechanistic Model Development. *J. Electrochem. Soc.* **1995**, *142*, 1–8. [CrossRef]
24. Wu, D.; Peng, C.; Yin, C.; Tang, H. Review of System Integration and Control of Proton Exchange Membrane Fuel Cells. *Electrochem. Energy Rev.* **2020**, *3*, 466–505. [CrossRef]
25. Mann, R.F.; Amphlett, J.C.; Hooper, M.A.I.; Jensen, H.M.; Peppley, B.A.; Roberge, P.R. Development and application of a generalised steady-state electrochemical model for a PEM fuel cell. *J. Power Sources* **2000**, *86*, 173–180. [CrossRef]

26. Li, Q.; Chen, W.; Wang, Y.; Jia, J.; Han, M. Nonlinear robust control of proton exchange membrane fuel cell by state feedback exact linearization. *J. Power Sources* **2009**, *194*, 338–348. [CrossRef]
27. Nguyen, T.V.; White, R.E. A Water and Heat Management Model for Proton-Exchange-Membrane Fuel Cells. *J. Electrochem. Soc.* **2019**, *140*, 2178–2186. [CrossRef]
28. Rowe, A.; Li, X. Mathematical modeling of proton exchange membrane fuel cells. *J. Power Sources* **2001**, *102*, 82–96. [CrossRef]
29. Pathapati, P.; Xue, X.; Tang, J. A new dynamic model for predicting transient phenomena in a PEM fuel cell system. *Renew. Energy* **2005**, *30*, 1–22. [CrossRef]
30. Sun, T.-S.; Chen, S.; Sun, H.; Li, J. Simulation analysis on thermal management characteristics of proton-exchange-membrane fuel-cell engine. *J. Chongqing Univ.* **2022**, 1–13. Available online: http://kns.cnki.net/kcms/detail/50.1044.N.20220105.1341.004.html (accessed on 23 December 2022).
31. Wang, Y.-X.; Qin, F.-F.; Ou, K.; Kim, Y.-B. Temperature Control for a Polymer Electrolyte Membrane Fuel Cell by Using Fuzzy Rule. *IEEE Trans. Energy Convers.* **2016**, *31*, 667–675. [CrossRef]
32. Tang, P.; Qi, Z.; Qian, M.; Yi, L. Temperature modeling and control of 5kW proton exchange membrane fuel cell system. In Proceedings of the IEEE International Conference on Information and Automation (ICIA), Ningbo, China, 1–3 August 2016.
33. Chen, F.; Yu, Y.; Gao, Y. Temperature Control for Proton Exchange Membrane Fuel Cell based on Current Constraint with Consideration of Limited Cooling Capacity. *Fuel Cells* **2017**, *17*, 662–670. [CrossRef]
34. Lin, Z. Research on Thermal Management System of Proton Exchange Membrane Fuel Cell. Master's Thesis, Beijing Jiaotong University, Beijing, China, 2021.
35. Han, J.; Yu, S.; Yi, S. Advanced thermal management of automotive fuel cells using a model reference adaptive control algorithm. *Int. J. Hydrogen Energy* **2017**, *42*, 4328–4341. [CrossRef]
36. Li, J. Thermal Management Design, Simulation and Optimization of Full-power Fuel Cell Vehicle Power System. Master's Thesis, Wuhan University of Technology, Wuhan, China, 2020.
37. Jin, L. Heat Transfer Model and Validation for Diesel Engine Cooling Systems of Heavy Duty Commercial Vehicles. Master's Thesis, Shanghai Jiao Tong University, Shanghai, China, 2010.